

**A NUMERICAL STUDY OF TRANSONIC BUFFET ON A SUPERCRITICAL AIRFOIL**

Q. Xiao<sup>1</sup> and H. M. Tsai<sup>2</sup>  
 Temasek Laboratories  
 National University of Singapore  
 Singapore 119260

F. Liu<sup>3</sup>  
 Department of Mechanical and Aerospace Engineering  
 University of California, Irvine CA 92697-3975

**Abstract**

The steady/unsteady flow of the BGK No. 1 supercritical airfoil is investigated by the solution of the Reynolds-Averaged Navier-Stokes equations with a two-equation  $k-\omega$  turbulence model. The dual-time stepping method is used to march in time. Two steady cases ( $Ma = 0.71, \alpha = 1.396^\circ$  and  $Ma = 0.71, \alpha = 9.0^\circ$ ) and one unsteady case ( $Ma = 0.71, \alpha = 6.97^\circ$ ), both with a far-stream  $Re = 20 \times 10^6$ , are computed. The results are compared with experimental data obtained by Lee et al. The mechanism of the self-excited oscillation for supercritical airfoils is explored. The oscillation period calculated based on the mechanism proposed by Lee is consistent with the Fourier analysis of the computed lift coefficient.

**Introduction**

Transonic buffeting flow appears in many aeronautical applications ranging from internal flows such as around turbo-machinery blades to flows over aircraft. Unsteady shock/boundary-layer interaction affects aerodynamic performance. For flows around an airfoil self-excited shock oscillations can cause flow separation and increase drag significantly. The capability to accurately predict such phenomena is of technological significance and a challenge. The accuracy of computation is influenced by both the accuracy of the numerical technique and the accuracy of the physically model, particularly, the turbulence model.

Self-excited oscillation has been investigated both experimentally and computational since the early work of McDevitt et al.<sup>1</sup> (e.g., Refs.1-18) Previous experimental and numerical studies of transonic flow over an 18% thick circular-arc airfoil have indicated that, the flow over a circular-arc aerofoil exhibit varied behavior depending on the flow conditions. Three distinct regions have been observed for a fixed free-stream Reynolds number but varying Mach number. Below a critical Mach number, the flow is steady and characterized by a weak shock wave near the mid-chord with trailing-edge flow separation. For larger Mach numbers, shock induced separation is encountered and the flow becomes unsteady, with unsteady shock motions on the upper and lower surface that are out of phase with each other. As the Mach number is further increased, a steady shock reappears. It is sufficiently strong to induce flow separation.

Compared to the non-lifting circular-arc airfoil, the study of other lifting supercritical airfoils is less matured. The computation and experiment of NASASC(2)-0714 have been reported in the paper of Bartels<sup>7</sup> and Bartels et al.<sup>8</sup>. An extensively set of data for the buffeting problem studied at the National Research Council, Canada of the flow over the Bauer-Garabedian-Korn (BGK) No. 1 supercritical airfoil at transonic speed has been reported by Lee<sup>9</sup>, Lee, et al.<sup>10</sup>, Lee<sup>11,12</sup>, and Lee, et al.<sup>13</sup>. The experiments were conducted over a range of Mach number and angle of attack. A map of the shock induced trailing edge separation regions together with steady and unsteady pressure measurements were reported for various shock/boundary-layer interactions. The investigation of the supercritical airfoil indicates, different from the circular-arc airfoil, the supercritical airfoil has a much weaker trailing edge separation in the onset region and experience shock oscillation only on one side of the airfoil.

The mechanism of the self-excited oscillation is not well understood although some explorations have been done by several researchers. (Refs. 11, 13-18). The investigation on the bi-convex airfoil suggested that the

---

1. Research Scientist, email: [tslxiaoq@nus.edu.sg](mailto:tslxiaoq@nus.edu.sg)  
 2. Principal Research Scientist, email: [tslthm@nus.edu.sg](mailto:tslthm@nus.edu.sg) Member AIAA.  
 3. Professor, email: [fliu@uci.edu](mailto:fliu@uci.edu) Associate Fellow AIAA.  
 Copyright © 2004 by the authors. Published by the American Institute of Aeronautics and Astronautics, Inc with permission

transonic periodic flows are initiated by an asymmetric unsteady disturbance. The shock induced separation changes the effective geometry of the airfoil, which would cause the forward and rearward movement of shock depending on whether the streamtube decreases or increases. The necessary but not sufficient condition for the periodic flow to appear is the shock wave strong enough to cause boundary separation. The Mach number just upstream of the shock should be in the range of  $1.14 < M_1 < 1.24$ . For the supercritical airfoil (Lee<sup>11</sup>), a model to predict the shock motion was formulated. The model assumed that the movement of shock leads to the formation of pressure waves which propagate downstream in the separated flow region. On reaching the trailing edge the disturbance generates upstream-moving waves, which interact with the shock wave and impart energy to maintain the limit cycle. The period of the oscillation should be the time for a disturbance to propagate from shock to the trailing edge plus the duration for an upstream moving wave to reach the shock from the trailing edge via the region outside the separated flow.

A number of difficulties are particular to the simulation of unsteady flow. Dual-time stepping method introduced by Jameson<sup>19</sup> provides an alternative to such direct computation of flow involving oscillation. This method uses an implicit physical time discretization. At each physical time step, the equations are integrated in a fictitious pseudo-time to obtain the solution to the steady state in pseudo-time. When marching in pseudo-time, this method permits the use of acceleration techniques such as local time step and multigrid to speed up the steady flows calculations. The application of dual-time stepping method of self-excited flow includes Rumsey et al.<sup>3</sup> and Oliver et al.<sup>5</sup> for the 18% circular-arc airfoil.

The assessment of turbulence models in unsteady aerodynamic flow featuring buffet and/or dynamic-stall has attracted less attention than the steady flow. In the early work of Levy<sup>2</sup>, computations were done using the Baldwin-Lomax<sup>20</sup> model which showed the unsteadiness in the flow field. It is sufficiently strong to induce flow separation. In terms of accuracy, the algebraic turbulence models such as the Baldwin-Lomax model do not perform well (Girodroux-Lavigne and LeBalleur<sup>14</sup>). Barakos & Drikakis<sup>6</sup> more recently presented an assessment of more advanced turbulence closures in transonic buffeting flows over airfoils. Various turbulence closures such as algebraic model, the one-equation model of Spalart and Allmaras<sup>21</sup>, the Launder-Sharma<sup>22</sup> and Nagano-Kim<sup>23</sup> linear k- $\epsilon$  models as well as the non-linear eddy-viscosity model of Craft et al.<sup>24</sup> and the non-linear k- $\omega$  model of

Sofialidis and Prinos<sup>25</sup> were studied with limited success.

One difficulty in most turbulence models is the inability to account directly for non-equilibrium effects found in separated flows. A new class of model was proposed by Olsen & Coakley<sup>26</sup>, which is termed the lag model. The basic idea of the lag model is to take a baseline two-equation model and couple it with a third (lag) equation to model the non-equilibrium effects for the eddy viscosity. Recently, Xiao et al.<sup>27</sup> incorporated the lag model with the baseline k- $\omega$  model and computed both steady and unsteady transonic nozzle flows. Their computations show notable improvements for strong shock cases, where strong non-equilibrium effect is present. For separated flows, good turbulence modeling is necessary to compute the overall flow physics. The lagged k- $\omega$  model also enjoys the advantage of not requiring specification of wall distance, and has similar or reduced computational effort compared with Reynolds stress models.

In the present work we employ the lag model coupled with the two-equation k- $\omega$  model for the study of transonic buffeting flow for the BGK No.1 supercritical airfoil, which is well documented in the paper of Lee<sup>9</sup>, Lee, et al.<sup>10</sup>, and Lee<sup>11,12</sup>. The computational results will be compared with the experiments for the steady/unsteady flow. The exploration of mechanism for the self-sustained oscillation will be conducted from the computational flow field. To the author's knowledge, no computational work has been done for this supercritical airfoil.

In the next section, the numerical implementation of the dual-time stepping method for the two-dimensional Navier-stokes equations will be briefly presented. The computational results and discussions will follow.

## **Numerical Method**

The governing equations for the unsteady compressible turbulent flow are expressed as follows:

Mass conservation:

$$\frac{\partial \rho}{\partial t} + \frac{\partial}{\partial x_j} (\rho u_j) = 0 \quad (1)$$

Momentum conservation:

$$\frac{\partial}{\partial t} (\rho u_i) + \frac{\partial}{\partial x_j} (\rho u_j u_i) = -\frac{\partial p}{\partial x_i} + \frac{\partial \hat{\tau}_{ji}}{\partial x_j} \quad (2)$$

Mean energy conservation:

$$\frac{\partial}{\partial t}(\rho E) + \frac{\partial}{\partial x_j}(\rho u_j H) = \frac{\partial}{\partial x_j} \left[ u_i \hat{\tau}_{ij} + (\mu + \sigma^* \mu_T) \frac{\partial k}{\partial x_j} - q_j \right] \quad (3)$$

Turbulent mixing energy:

$$\frac{\partial}{\partial t}(\rho k) + \frac{\partial}{\partial x_j}(\rho u_j k) = \tau_{ij} \frac{\partial u_i}{\partial x_j} - \beta^* \rho \omega k + \frac{\partial}{\partial x_j} \left[ (\mu + \sigma^* \mu_T) \frac{\partial k}{\partial x_j} \right] \quad (4)$$

Specific dissipation rate:

$$\frac{\partial}{\partial t}(\rho \omega) + \frac{\partial}{\partial x_j}(\rho u_j \omega) = (\varepsilon \omega / k) \tau_{ij} \frac{\partial u_i}{\partial x_j} - \beta \rho \omega^2 + \frac{\partial}{\partial x_j} \left[ (\mu + \sigma \mu_T) \frac{\partial \omega}{\partial x_j} \right] \quad (5)$$

Turbulent eddy viscosity:

$$\frac{\partial}{\partial t}(\rho \nu_t) + \frac{\partial}{\partial x_j}(\rho u_j \nu_t) = a(R_T) \omega \rho (\nu_{tE} - \nu_t) \quad (6)$$

where  $t$  is time,  $x_i$  position vector,  $\rho$  is the density,  $u_i$  velocity vector,  $p$  pressure,  $\mu$  dynamic molecular viscosity,  $\nu_{tE}$  kinematic equilibrium turbulent eddy viscosity,  $k$  turbulent mixing energy, and  $\omega$  the specific dissipation rate. The total energy and enthalpy are  $E = e + k + u_i u_i / 2$  and  $H = h + k + u_i u_i / 2$ , respectively, with  $h = e + p / \rho$  and  $e = p / [(\gamma - 1) \rho]$ . The term  $\gamma$  is the ratio of specific heats. Other quantities are defined in the following equations:

$$\mu_T = \rho \nu_t \quad (7)$$

$$\nu_{tE} = \varepsilon^* k / \omega \quad (8)$$

$$R_T = \rho k / \mu_T \omega \quad (9)$$

$$S_{ij} = \frac{1}{2} \left( \frac{\partial u_i}{\partial x_j} + \frac{\partial u_j}{\partial x_i} \right) \quad (10)$$

$$\tau_{ij} = 2\mu_T (S_{ij} - \frac{1}{3} \frac{\partial u_k}{\partial x_k} \delta_{ij}) - \frac{2}{3} \rho k \delta_{ij} \quad (11)$$

$$\hat{\tau}_{ij} = 2\mu (S_{ij} - \frac{1}{3} \frac{\partial u_k}{\partial x_k} \delta_{ij}) + \tau_{ij} \quad (12)$$

$$q_j = - \left( \frac{\mu}{Pr_L} + \frac{\mu_T}{Pr_T} \right) \frac{\partial h}{\partial x_j} \quad (13)$$

$$a(R_T) = a_0 \left[ \frac{(R_T + R_{T0})}{(R_T + R_{T\infty})} \right] \quad (14)$$

Where  $Pr_L$  and  $Pr_T$  are the laminar and turbulent Prandtl numbers, respectively. The other coefficients are:

$$a_0 = 0.35, \quad R_{T0} = 1, \quad R_{T\infty} = 0.01, \quad \varepsilon = 5/9, \quad \varepsilon^* = 1, \quad \beta = 0.075, \quad \beta^* = 0.09, \quad \sigma = 0.5, \quad \sigma^* = 0.5.$$

It is known that conventional one- and two-equation turbulence models generate Reynolds stresses that respond too rapidly to changes in mean flow conditions partially due to the need to accurately reproduce equilibrium flows. As a result, these baseline turbulence models give unsatisfactory results for flows with significant separation under adverse pressure gradients or across shock waves. In the present computation, the standard k- $\omega$  turbulence model is coupled with the lag model proposed by Olsen and Coakley<sup>26</sup> to calculate the turbulent eddy viscosity.

The basic numerical method used to solve the above system of equations in this paper follows that described in detail by Liu and Ji<sup>28</sup>. The integral forms of the conservation equations are discretized on quadrilateral cells using the finite volume approach. A staggered scheme is used for the coupling of the Navier-Stokes equations and the k- $\omega$  and lag equations. A central difference scheme is used to discretize the diffusive terms and an upwind Roe's scheme is used for convective terms in the Navier-Stokes and the k- $\omega$  equations.

After being discretized in space, the governing equations are reduced to a set of ordinary differential equations with only derivatives in time, which can be solved using a multi-stage Runge-Kutta type scheme. To accelerate the convergence, unsteady multigrid method proposed by Jameson<sup>19</sup> and further implemented by Liu and Ji<sup>28</sup> is applied in the present study for all 7 equations.

## **Results and Discussions**

The numerical method presented above is applied to the Bauer-Garabedian-Korn (BGK) No. 1 supercritical airfoil which is extensively investigated experimentally at the National Research Council, Canada. The geometry of the airfoil is shown in Fig. 1. The experiments have been conducted at a chord Reynolds number of  $20 \times 10^6$  with free transition. The Mach numbers in the investigation ranged from 0.5 to 0.792 with angle of attack  $\alpha$  varying from 1.3 to 11.5 degree. It is reported, from the force and pressure power spectrum, strong shock oscillation occurs for Mach

numbers between 0.69 and 0.733. For the present numerical simulation, three test cases are conducted with a fixed chord Reynolds number of  $20 \times 10^6$  and Mach number of 0.71 at three different angles of attack, case 1:  $\alpha = 1.396^\circ$ ; case 2:  $\alpha = 6.97^\circ$ ; and case 3:  $\alpha = 9.0^\circ$ . Based on Lee's experimental results, the flow is steady for the flow conditions of case 1 and case 3. For case 2, however the flow is unsteady with shock induced oscillation. It should be noted that the Mach number and angle of attack used in the computation are the same as the experimental ones without any wind tunnel correction.

The computational grid has a C-topology. Most of the computations are performed on a  $640 \times 64$  mesh with 512 points on the surface of the airfoil, 128 nodes in the wake. The computational domain extends approximately 20 chords up and down stream. The average minimum normal spacing at the wall is approximately  $10^{-6}$  chord, which corresponds to a  $y^+$  value of about 0.6 for an unsteady calculation at  $Ma = 0.71$  with  $\alpha = 6.97^\circ$ . The grid independence test has been conducted and the results will be presented in detail later.

The no slip boundary conditions are imposed on the airfoil surface. At the outer boundary, far-field Riemann invariant boundary conditions are employed and at the downstream all variables are extrapolated.

Most of the calculation starts from a uniform free-stream flow field. All three cases are computed using three levels of multigrids with CFL number varying from 3.0 to 7.0.

Figure 2 shows the evolution of the lift coefficient  $Cl$  for  $Ma = 0.71$  and  $\alpha = 1.396^\circ$  with the computation starting from the uniform flow. The computed  $Cl$  approaches a constant around 0.7 after a few iterations, which indicates the flow is steady without the shock-induced oscillation. The Mach contours shown in Fig. 3 reveals a weak shock formed at about one quarter of the airfoil, but without flow separation. The pressure coefficient distribution along the airfoil upper surface is shown in Fig. 4 as well as the experimental data of Lee<sup>10</sup>. The computation is generally in good agreement with the experiment except the shock location predicted is too downstream compared to the experiment. This is possibly due to the wind tunnel wall effect. In the computation, no wind tunnel correction is used.

For case 2 with  $Ma = 0.71$  and  $\alpha = 6.97^\circ$ , the  $Cl$  evolution is presented in Fig. 5. The flow at these

conditions develops into unsteady with shock-induced oscillation. The average lift coefficient is 1.03 which is close to the experimental data of 1.016. Fourier analysis result shown in Fig. 6 reveals a predominant reduced frequency ( $k = \pi fc / U_\infty$ ) equal to 0.16, which is about 0.4 of the bi-convex circular airfoil. This value is about 60% lower than the experimental value of Lee<sup>10</sup>.

The Mach number contours and skin friction coefficient  $Cf$  plots at different time instants during one oscillation period are presented in Fig. 7. The instantaneous shock positions on the upper surface of the airfoil are shown in Fig. 8. The  $t^*$  equal to zero corresponds to the time instant at which the lift coefficient  $Cl$  is the minimum. Both Fig. 7 and Fig. 8 reveal that, different from the non-lifting bi-convex circular-arc airfoil, the shock oscillation here occurs on the upper side of the airfoil only. The shock motion is mainly of the type A reported by Tijdeman<sup>29</sup>. Detailed flow features can be obtained from the Mach number contours and the skin friction distributions in Fig. 7. At  $t^* = 0$ , a weak shock occurs at a location of approximately one quarter of the airfoil, and there is a small separation region after the shock. During the first half cycle ( $0 < t^* < 0.5$ ), the shock becomes stronger and moves down-stream with time increasing. This is typified in Fig. 7 for  $t^* = 0.2$  and  $t^* = 0.4$ . A larger flow separation can be spotted from the  $Cf$  plot at  $t^* = 0.4$ . The shock reaches the most rearward position at about  $t^* = 0.5$  which is followed by a forward movement of the shock in the second half of the cycle ( $0.5 < t^* < 1.0$ ). The separation region continues to increase until the shock reaches the most forward position at about  $t^* = 0.8$ . The shock strength, however continues to decrease during this period which is indicated from the change of normal shock at  $t^* = 0.4$  to oblique shock at  $t^* = 0.8$ . Subsequently, the shock moves rearwards with a decreasing separation region.

The time-mean pressure distribution ( $-Cp$ ) along the upper surface of the wall is shown in Fig. 9 as well as the experimental data of Lee. The computation as seen is in good agreement with the experiment.

The variation of top wall pressure distribution ( $-Cp$ ) due to shock oscillation within one cycle is shown in Fig. 10 for different locations of the airfoil upper surface (E to T corresponding to Lee's experiment indicated in Fig. 1). The computation is comparable to the experimental results of Lee (see Ref. 11 Fig. 9).

The amplitude and phase angle of the unsteady pressure on the upper surface of the airfoil are presented in Fig. 11 and Fig. 12 as well as the experimental data. The distinguishable difference is observed from Fig. 11. The

computations show an increase in amplitude with increasing  $x/c$  for  $x/c < 0.4$ , subsequently a decrease with increasing  $x/c$  within the range of  $0.4 < x/c < 0.6$ , and then remain a constant. The experiments, however show the continuous decreasing of amplitude before  $x/c < 0.4$ , then slightly increase and decrease with  $x/c$ . From Fig. 12, a similar trend is observed for the phase angle plot between experiment and computation except that, the computational values are slightly larger than the experiments. Both results show a linear relationship between phase angle and stream-wise location after  $x/c > 0.5$ . This indicates the pressure wave propagates down stream with a constant velocity.

Fig. 13 shows the evolution of the lift coefficient  $Cl$  for case 3, i.e.:  $Ma = 0.71$  and  $\alpha = 9.0^\circ$ . The  $Cl$  plot indicates the flow becomes steady again. The Mach number contours and top wall pressure distribution are presented in Figs. 14 and 15, respectively. The shock is near the leading edge and a strong separation extends to the trailing edge.

## DISCUSSION

### Influence of mesh

An investigation of the influence of the mesh on the solution has been conducted for the unsteady calculation at  $Ma = 0.71$  with  $\alpha = 6.97^\circ$ . The fine grid has  $640 \times 64$  points, the medium  $552 \times 48$ , and the coarse grid  $320 \times 32$ . Comparisons of time-history of the lift coefficient, reduced frequency, and time-mean pressure distribution are shown in Figs. 16-18.

Large discrepancies exist between the solution on the coarse grid and those on the fine grids for the time history of  $Cl$  and the pressure distributions although the predominant reduced frequency is not sensitive to the grid. This indicates that the  $320 \times 32$  grid is not sufficient to correctly predict the flow field. For the medium and fine grid, the difference is small except the shock captured by the fine grid solution appears to be sharper than that by the medium grid and close to the experiment.

### Influence of the initial condition

As the initial conditions are different in the experiments and the computations, it is important to investigate their influence on the characteristics of the computed unsteady buffeting flows. Two test cases were carried out for  $Ma = 0.71$  and  $\alpha = 6.97^\circ$ . One starts from a uniform flow, the other starts from a converged steady solution for  $Ma = 0.71$  and  $\alpha = 1.396^\circ$ . The comparison for the evolution of lift coefficient  $Cl$  shown in Fig. 19 reveals that the time for the flow to reach a periodic solution is earlier for the calculation initialized with the

converged steady result. The time-mean lift coefficient and oscillation frequency are found to be the same for the two cases. The time-mean pressure distributions are also the same (shown in Fig. 20).

### Influence of the lag model

To evaluate the lag model performance, the computation with the base-line  $k-\omega$  model without the lag model is conducted for the unsteady flow of  $Ma = 0.71$  and  $\alpha = 6.97^\circ$ . The lift coefficient development, Fourier analysis of oscillation, and the time-mean pressure distribution are shown in Figs. 21-23, respectively. From Fig. 21,  $Cl$  oscillation obtained without the lag model takes longer time to be stable than that with the lag model for the same CFL and multigrid number. In addition, the average  $Cl$  value without the lag model is larger than the result with the lag model and therefore divergent more from the experiment  $Cl = 1.016$ . The Fourier analysis shows a similar dominant reduced frequency ( $k = \pi f c / U_\infty$ ) of 0.16. The comparison of computational time-mean pressure distribution with the experiment clearly reveals the solution with the lag model is much better than the solution without the lag model. It is noted from experiment, the unsteady flow at this condition is fully separated. The computation verifies again the lag model performs better than the base-line  $k-\omega$  model when strong separation appears.

### Mechanism of the shock induced oscillation

In the paper of Lee<sup>11</sup>, an explanation of the mechanism of self-sustained shock oscillation and a method to estimate the frequency of oscillation were given. The model assumed that the flow behind the shock boundary-layer interaction to be fully separated. Pressure waves, formed as a result of the movement of the shock, propagate downstream in the separated flow region (see Fig. 24). On reaching the trailing edge, the disturbances generate upstream-moving waves in the region outside the separated flow as a result of satisfying the unsteady ‘‘Kutta’’ condition. The upstream-moving wave interacts with the shock, and impart energy to return it to its initial location. The loop is then completed. The period of the shock oscillation is the time it takes for a disturbance to propagate from the shock to the trailing edge plus the duration for an upstream wave to reach the shock from the trailing edge (see Lee et al.<sup>13</sup>). This is given by the following formulation (Lee<sup>11</sup>):

$$T_p = T_{p1} + T_{p2} \quad (15)$$

$$T_{p1} = \int_{x_s}^c 1/a_p dx \quad (16)$$

where  $T_{p1}$  is the time for the downstream pressure wave propagation,  $T_{p2}$  the time for the upstream wave

and  $a_p$  is the velocity of the downstream pressure wave in the separated flow region. The  $a_p$  can be calculated from the pressure wave phase angle versus  $x/c$  relation. For the time taken by a disturbance to travel from the trailing edge to the shock ( $T_{p2}$ ), there are several methods available. The first uses the empirical formula given by Erickson and Stephenson<sup>30</sup> as follows:

$$f = \frac{a(1-M)}{4(c-x_s)} \quad (17)$$

where  $c$  is the chord length,  $a$  the far-stream sound speed,  $M$  the far-stream Mach number and  $f$  the frequency of the upstream wave.  $T_{p2}$  is then determined by  $T_{p2} = 1/f$ . Mabey<sup>31</sup> computed the reduced frequency ( $2\pi fc/U_\infty$ ) using Eq. (17), the result is approximately 1.43 compared to about 1 from experiments.

The second method to determine  $T_{p2}$  is based on the assumption of Tijdeman<sup>29</sup>. Optical studies of self-sustained oscillation show that the wake oscillates in a synchronous manner with the shock oscillations and behaves like a flap. Tijdeman<sup>29</sup> has pointed out that the flap can be treated as an acoustic source placed at the hinge line, and the time required for a disturbance to travel from the trailing edge to the shock is given by the following expression:

$$T_{p2} = \int_c^{x_c} \frac{dx}{(1-M_{loc})a_{loc}} \quad (18)$$

where  $M_{loc}$  and  $a_{loc}$  are the local Mach number and speed of sound, respectively.  $M_{loc}$  is approximated by the following empirical formula:

$$M_{loc} = R[M_{loc-s} - M_\infty] + M_\infty \quad (19)$$

where  $M_{loc-s}$  and  $M_\infty$  are the Mach number at the surface and far stream, respectively, and  $R$  is 0.7.

Lee<sup>11</sup> expressed Eq.(18) in the following form:

$$T_{p2} = \int_c^{x_c} 1/a_u dx \quad (20)$$

where  $a_u$  is the velocity of the upstream wave outside the separated region. As this value is not easily measured experimentally, Lee et al.<sup>13</sup> estimated it using the empirical formula given by Tijdeman<sup>29</sup> as:

$$a_u = (1-M_{loc})a_{loc} \quad (21)$$

Mabey et al.<sup>32</sup> related Eqs. (18-19) with reduced frequency and found the values were 3.6 and 2.3 for  $M = 0.81$  and  $M = 0.88$  which are higher than the experimental data of about 1.0. The accuracy of the use

of Tijdeman<sup>29</sup> formula is accessed by Lee et al.<sup>13</sup>. The propagation of pressure disturbance is analyzed by the nonlinear transonic small disturbance equation. The results for the NACA 64A006 airfoil compare favorably with the numerical computations when the integration of the Eq. (20) is carried out on a line starting at the trailing edge at 170 deg angle. In the paper of Lee<sup>11</sup>, the method is used to estimate the oscillation frequency for the BGK No.1 supercritical airfoil, their calculated frequency is found to be fair with the measured shock oscillation frequency from the balance force spectra. That provides evidence for the possible mechanism of self-sustained shock oscillation proposed by Lee<sup>11</sup>.

In the present study, the above mechanism has been explored using the computational results. Two-point pressure cross correlation are used to determine the propagation direction of the pressure fluctuations. For the separated flow region, the cross correlation analysis is conducted for the upper surface pressure at the points from E to T, (shown in Fig.1). The point nearest the trailing edge (T) is used as the reference in each cross correlation. For the outside separation region, pressure cross correlation are done for points A to D using A as the reference (shown in Fig. 25). The results are shown in Figs. 26 and 27, respectively. Inside the separated region, the cross correlation in Fig. 26 shows that the surface pressure disturbances propagate downstream from shock to the trailing edge. However, negative time delay is observed in Fig. 27 for the pressure outside the separation region, which indicates that the disturbances are moving upstream. This appears to be consistent with the hypothesis of Lee<sup>11</sup>.

The shock oscillation period is calculated by using Eq. (15) and the time of downstream pressure wave propagation ( $T_{p1}$ ) is obtained by Eq. (16). The value of  $a_p$  is computed from the pressure wave phase angle versus  $x/c$  relation shown in Fig. 12. The almost linear relation can be seen for  $x/c > 0.25$  and the average velocity of the pressure wave for this particular figure is about  $0.12 U_\infty$ .

The time for upstream wave propagation from the trailing edge to the shock is calculated by two methods. The first (Method 1) uses Eq. (17), which is independent of the local flow field, but is related to the far stream Mach number and sound speed only. The time-mean shock location  $x_s$  is about 0.15 chord for  $Ma = 0.71$  and  $\alpha = 6.97^\circ$ . The second method (Method 2) uses Eq (20). Different from Lee<sup>11</sup>'s method, the upstream wave velocity ( $a_u$ ) here is calculated from

the above pressure correlations of the computed results instead of the empirical formula of Eqns. (19) and (21). The average propagation speed  $a_u$  is obtained in a cross correlation by using the spatial separation between the points and the time delay corresponding to the correlation peak. Results for the calculated reduced frequency ( $k = 2\pi fc/U_\infty$ ) by the two methods are given in Table one as well as the Fourier analysis result of lift coefficient Cl. It should be pointed out that, in the experiment the oscillation frequency is derived from the normal force spectra. However, this value is obtained from the Fast Fourier Transformation of Cl in the CFD. It is treated as the basis for the comparison with the computation from Method 1 and Method 2.

Table 1. Comparison of reduced frequency obtained by different method.

Method 1	Method 2	FFT result
0.41	0.39	0.32

Both computations with Method 1 and 2 are close to the Fourier analysis result for Cl. The good agreement indicates the validity of Eq. (15), i.e.: the oscillation period is equal to the sum of the time for a disturbance traveling from shock to the trailing edge and the time of the disturbance propagating from the trailing edge to the shock. This provides strong evidence to the mechanism of self-sustained oscillation proposed by Lee.

To gain further insight into the unsteady flow features, the streamline plots near the trailing edge at different time instants during one oscillation cycle are shown in Fig. 28. The separated flow region at  $t^*=0$  extends from  $x/c=0.65$  on the airfoil to  $x/c=1.35$  in the wake region. At subsequent time instants, the separation location moves downstream, and the separated flow convects downstream and eventually disappears on the top region of the airfoil about the time from  $t^*=0.1$  to 0.2. At a later time separated flow reappears and a bulge can be observed around  $x/c=0.55$  at  $t^*=0.3$  which then forms a new vortex. At the time instants of  $t^*=0.4$  and 0.5, the bulge becomes larger and a new separation region appears at  $t^*=0.5$ . This also corresponds to the instants of maximum lift. In the subsequent time instants ( $t^*=0.6, 0.7$  and 0.8), this vortex increases its size in both upstream and downstream directions with a corresponding loss of lift. A secondary vortex is also formed in the vicinity of the trailing edge at  $t^*=0.7$  and 0.8. The vortices coalesce and form one large separation flow region which decreases in size in the successive time instant  $t^*=0.9$ . The cycle of separated flow and shock movement then repeats itself.

It is thought that the shock induced oscillation on the airfoil is initiated by an unsteady asymmetric disturbance and sustained by the communication across the trailing edge. From the above results and discussion, it is best described as the case where the disturbance is caused by the formation of the separation bubble which is inherently unsteady as it interacts with the shock wave. The unstable separation bubble changes the effective geometry of an airfoil similar to the effect of a trailing edge flap oscillating upwards in a periodic manner. The separated flow being a low momentum flow region reduces the effective chamber and hence the resulting reduction of lift. The separated flow also creates an upstream wave, which provides the feedback from the rear of the airfoil to perturb the shock upstream. This mechanism can be self sustaining as we have seen in this case of the BGK supercritical airfoil at  $Ma=0.71$  and angle of attack at 6.97 degrees.

## Conclusions

The computation of self-excited oscillation on BGK No. 1 supercritical airfoil is conducted using the lagged two-equation  $k-\omega$  turbulence model. This work appears to be the first for modeling the BGK. No. 1 supercritical airfoil. The results are presented and compared with experimental data. The mechanism of the shock oscillation is also investigated. The main conclusions can be drawn as follows:

- 1) The unsteady results are generally in good agreement with experiment except the oscillation frequency is lower than that of experiment.
- 2) The calculations of oscillation frequency based on the suggestion of Lee<sup>12</sup> are close to the FFT result of lift coefficient Cl. This provides solid evidence to the mechanism of self-sustained oscillation by Lee<sup>11</sup>.
- 3) For the fully separated unsteady flow of  $Ma = 0.71$  and  $\alpha = 6.97^\circ$ , notable improvement can be observed by using the lag model on the surface pressure distribution and lift coefficient. For the oscillation frequency, the impact is small.

## REFERENCES

1. McDevitt, J.B. Levy, L.L. and Deiwert, G.S. "Transonic flow about a thick circular-arc airfoil," *AIAA Journal*, Vol.14, No.5, 1976, pp.606-613.
2. Levy L.L. "Experimental and computational steady and unsteady transonic flows about a thick airfoil," *AIAA Journal*, Vol.16, No.6, 1978, pp.564-572.
3. Rumsey, C.L., Sanetrik, M.D., Biedron, R.T., Melson, N.D. and Parlette, E.B. "Efficiency and accuracy of time-accurate turbulent Navier-Stokes computation," *Computers & Fluids*, Vol. 25, No.2, 1996, pp. 217-236.
4. Edwards, J.W. "Transonic shock oscillations calculated with a new interactive boundary layer coupling method" AIAA-93-0777.
5. Oliver, R. Stylvie, P. and Vincent, C. "Numerical simulation of buffeting over airfoil using dual time-stepping method" European congress on computational methods in applied science and engineering ECCOMAS 2000.
6. Barakos, G., Drikakis, D., "Numerical simulation of transonic buffet flows using various turbulence closures," *Int. J. Heat and Fluid Flow*, Vol. 21, 2000, pp.620-626.
7. Bartels, R.E., "Flow and turbulence modeling and computation of shock buffet onset for conventional and supercritical airfoils" NASA/TP-1998-206908.
8. Bartels, R. E., Robert, E., Edwards and John, W. "Cryogenic tunnel pressure measurements on a supercritical airfoil for several shock buffet conditions" NASA TM-110272, 1997.
9. Lee, B.H.K. "Transonic buffet on a supercritical airfoil." *Aeronaut. J.* May, 1990, pp. 143-152.
10. Lee, B.H.K., Ellis, F.A. and Bureau, J. "Investigation of the buffet characteristics of two supercritical airfoils" *J. Aircraft*, Vol. 26, No. 8, 1989, pp. 731-736.
11. Lee, B.H.K. "Oscillation shock motion caused by transonic shock boundary layer interaction" *AIAA J.* Vol. 28, No. 5, 1990, pp. 942-944.
12. Lee, B.H.K. "Self-sustained shock oscillations on airfoils at transonic speeds" *Progress in Aerospace Sciences*, Vol. 37, 2001, pp. 147-196.
13. Lee, B.H.K., Murty, H. and Jiang, H. "Role of Kutta waves on oscillatory shock motion on an airfoil" *AIAA J.* Vol. 32, No.4, 1994, pp. 789-795.
14. Girodroux-Lavigne, P., LeBalleur J.C., "Time consistent computation of transonic buffet over airfoils" 1988, ONERA TP No. 1988-97.
15. Mabey, D.G., "Physical phenomena associated with unsteady transonic flow," Chapter 1 in *Unsteady transonic aerodynamics*, ed. by D.Nixon, Vol.120 in *AIAA Progress in Aeronautics and Astronautics*, 1989.
16. Raghunathan, S, Hall, D.E., Mabey, D.G., "Alleviation of shock oscillations in transonic flow by passive control. *Aeronaut. J.*, Vol. 94, No. 937,1990, pp. 245-250.
17. Raghunathan, S, Zarifi-Rad, F, Mabey, D.G., "Effect of model cooling in transonic periodic flow" *AIAA J.*, Vol. 30, No. 8,1992, pp. 2080-2089.
18. Gibb, J. "The cause and cure of periodic flows at transonic speeds." *Proceedings 16<sup>th</sup> Congress of the International Council of the Aeronautical Sciences, Jerusalem, Israel, August-September, 1988*, pp. 1522-1530.
19. Jameson, A., "Time dependent calculations using multigrid, with applications to unsteady flows past airfoils and wings," *AIAA Paper 91--1596*, 10th *AIAA Computational Fluid Dynamics Conference*, Jun, 1991.
20. Baldwin, B.S., Lomax, H., "Thin layer approximation and algebraic model for separated turbulent flows," *AIAA Paper 78-257*,1978.
21. Spalart, P.R, Allmaras, S.R., "A one-equation turbulence model for aerodynamic flows" *AIAA 92-0439*,1992.
22. Launder, B.E., Sharma, B.I., "Application of the energy-dissipation model of turbulence to the calculation of flow near a spinning disk," *Lett. Heat Mass Transfer* Vol. 1, 1974, pp.131-138.
23. Nagano, Y., Kim, C., "A two equation model for heat transport in wall turbulent shear flows." *J. Heat Transfer*, Vol.110, pp.583-589. 1988
24. Craft, T.J., Launder, B.E., Suga, K., "Development and application of a cubic eddy-viscosity model of turbulence". *Int. J. Heat Fluid Flow*, Vol.17, 1996. pp.108-115.
25. Sofialidis, D., Prinos, P., "Development of a non-linear strain sensitive k- $\omega$  turbulence model," In: *Proceedings of the 11<sup>th</sup> Symposium on Turbulent Shear Flows, TSF-11*, Grenoble, France, p2-89-p2-94. 1997.
26. Olsen, M.E. and Coakley, T.J., "The lag model, a turbulence model for non-equilibrium flows," *AIAA 2001-2564*, 2001.
27. Xiao, Q., Tsai, H.M. and Liu, F., "Computation of transonic diffuser flows by a

- lagged  $k-\omega$  turbulence model,” *Journal of Propulsion and Power*, vol. 19, no. 3, May-June, 2003, pp. 473-483.
28. Liu, F. and Ji, S., “Unsteady flow calculations with a multigrid Navier-Stokes Method,” *AIAA Journal*, Vol. 34, No. 10, 1996, pp. 2047-2053.
  29. Tijdeman, H., “Investigation of the transonic flow around oscillation airfoils” NLR TR 77090 U, National Aerospace Laboratory, The Netherlands, 1977.
  30. Erickson, A.L., Stephenson, J.D., “A suggested method of analyzing transonic flutter of control surfaces based on available experimental evidence.” NACA RM A7F30, National Advisory Committee for Aeronautics, December 1947.
  31. Mabey, D.G., “Oscillatory flows from shock-induced separations on biconvex airfoils of varying thickness in ventilated wind tunnels.” AGARD CP-296, Boundary layer effects on unsteady airfoils, Aix-en-Provence, France, 14-19 Sept. 1980, pp.11.1-14.
  32. Mabey, D.G., Welsh, B. L. and Cripps, B. E. “Periodic flows on a rigid 14% thick biconvex wing at transonic speeds.” TR81059, Royal Aircraft Establishment, May 1981.

TRANSDUCER: E F G H I J K L  
 x (inches): 2 2.5 3 3.5 4 4.5 5 5.5  
 TRANSDUCER: M N O P Q R S T  
 x (inches): 5.91 6.32 6.73 7.14 7.55 7.96 8.37 8.7

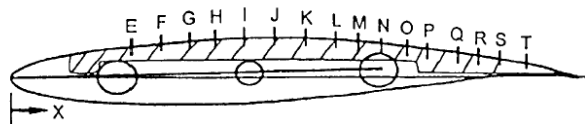


Fig.1 Geometry of the BGK No.1 supercritical airfoil. (From Ref. 9)

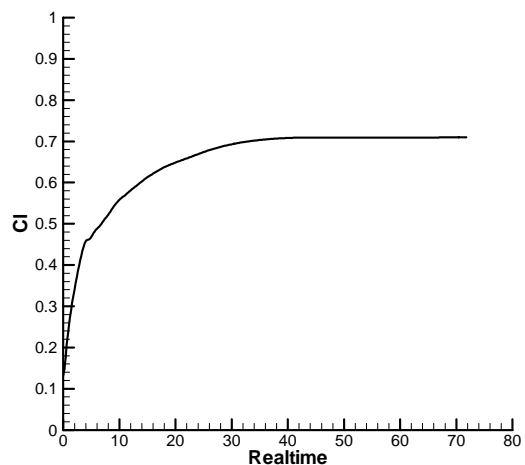


Fig.2 Evolution of lift coefficient  $C_l$  of  $Ma = 0.71$  and  $\alpha = 1.396^\circ$ .

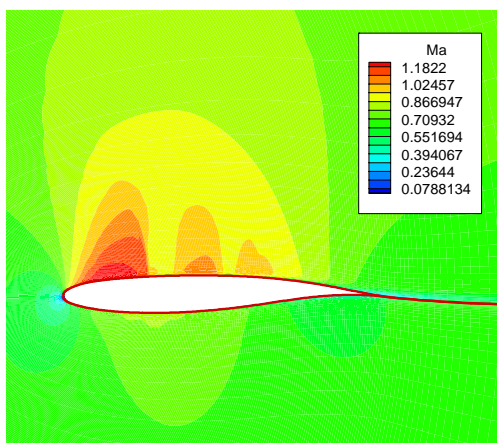


Fig. 3 Mach contour of  $Ma = 0.71$  and  $\alpha = 1.396^\circ$ .

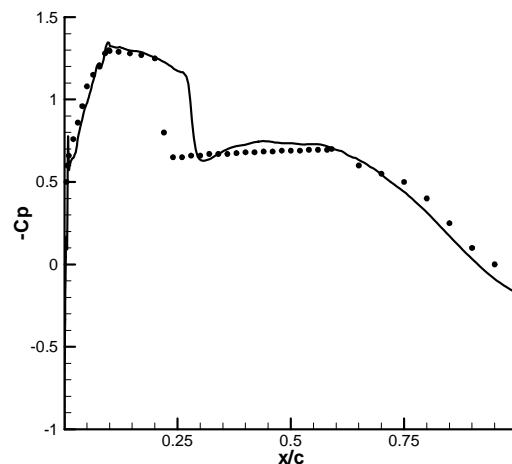


Fig. 4 Pressure distribution along the upper surface of airfoil.  $Ma = 0.71$  and  $\alpha = 1.396^\circ$ .

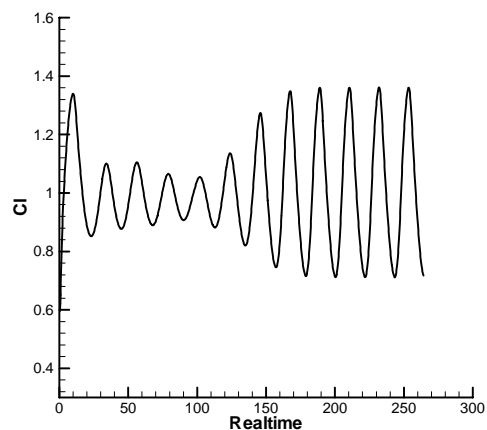


Fig. 5 Evolution of lift coefficient  $C_l$  of  $Ma = 0.71$  and  $\alpha = 6.97^\circ$ .

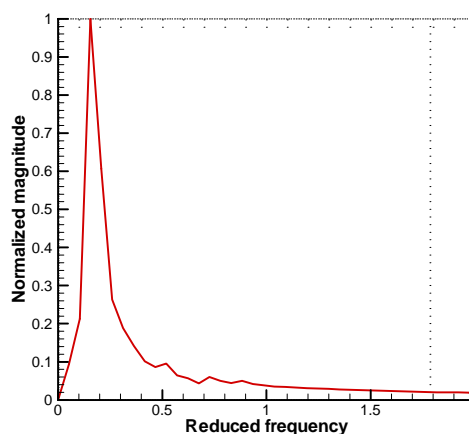


Fig. 6 Fourier analysis of reduced frequency for  $Ma = 0.71$  and  $\alpha = 6.97^\circ$ .

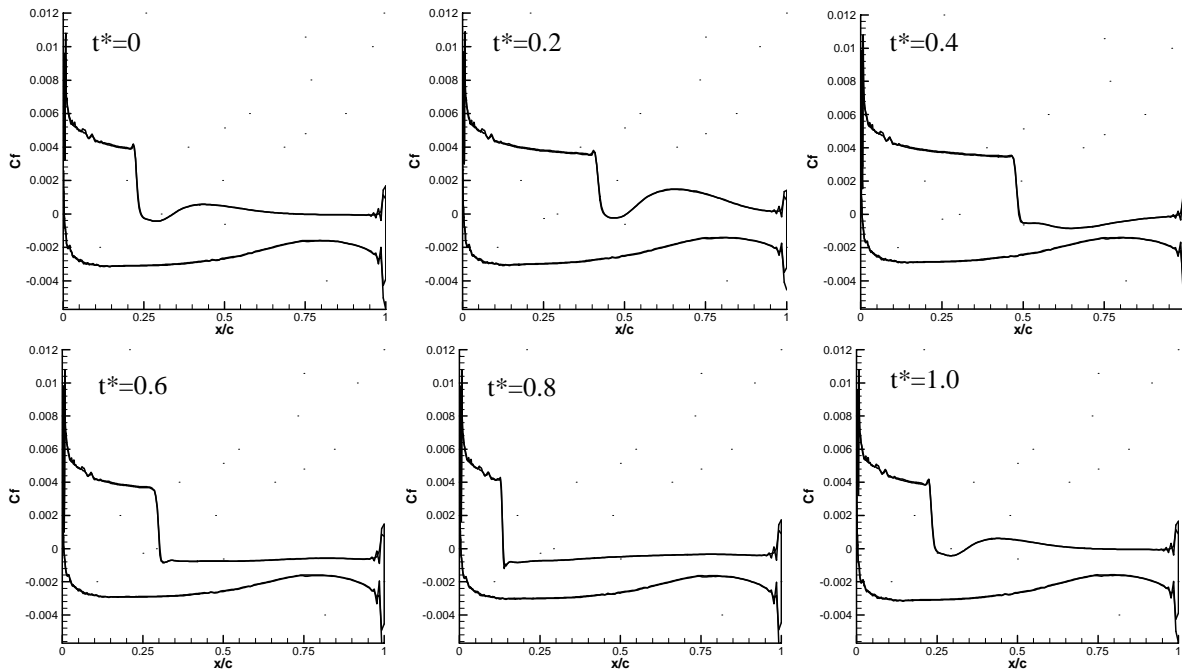
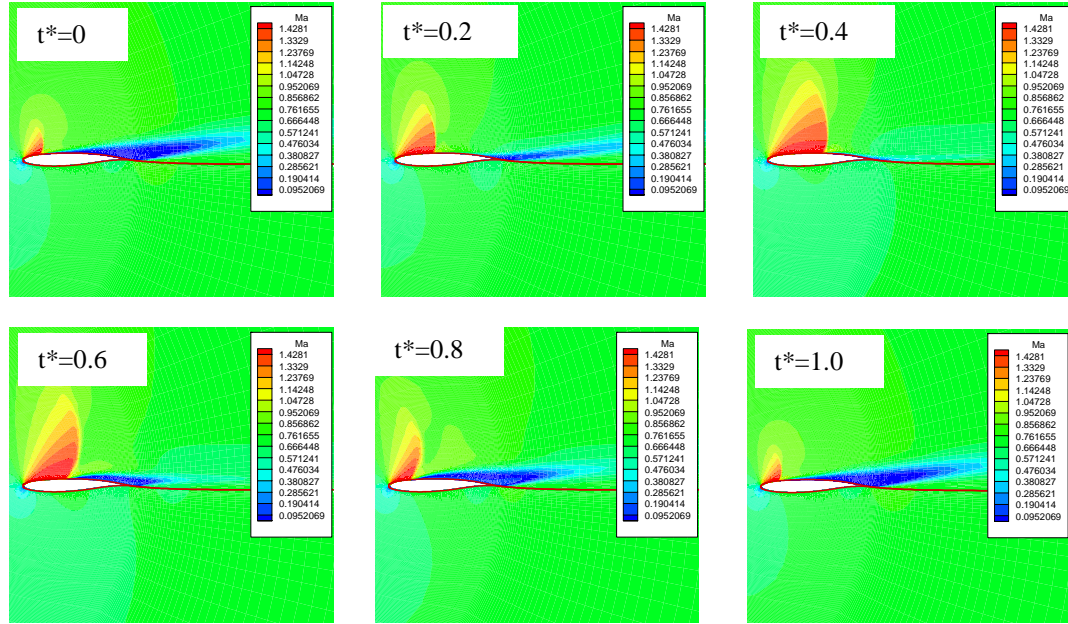
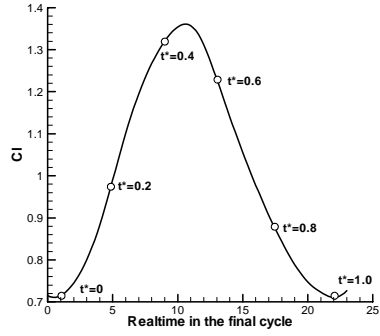


Fig. 7 Mach number contour and skin coefficient at different instant time in one period.  $Ma = 0.71$  and  $\alpha = 6.97^\circ$ .

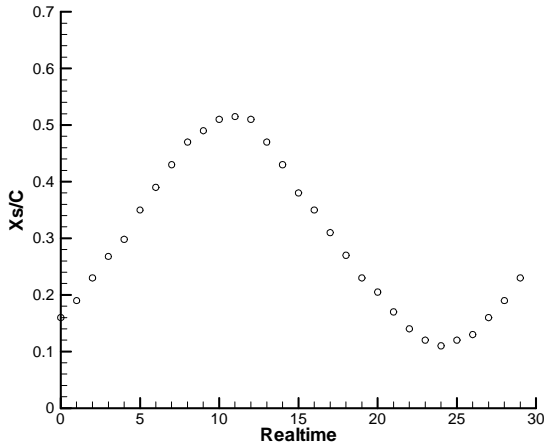


Fig. 8 Shock position in one oscillation cycle.

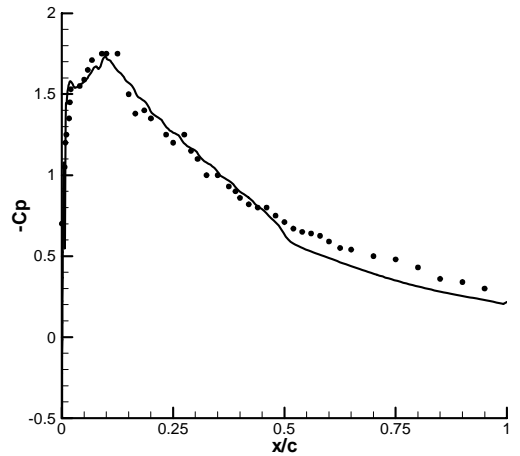


Fig. 9 Time-mean pressure comparison with experimental results. Closed circle: experiment; Line: computation.

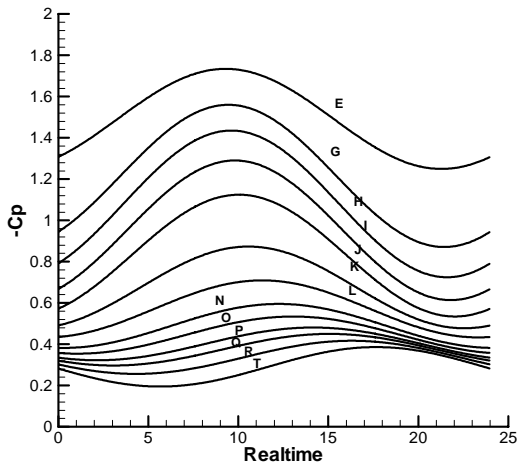


Fig. 10 Pressure distribution vs time at the different location of upper surface due to shock oscillation.

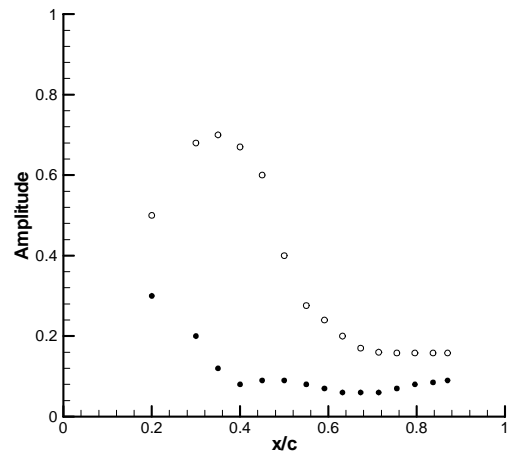


Fig. 11 Amplitude of unsteady pressure on airfoil. Closed circle: experiment; open circle: computation.

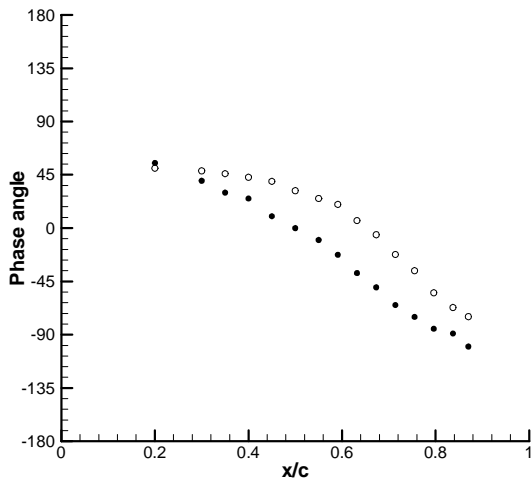


Fig. 12 Phase angle of unsteady pressure on airfoil. Closed circle: experiment; open circle: computation

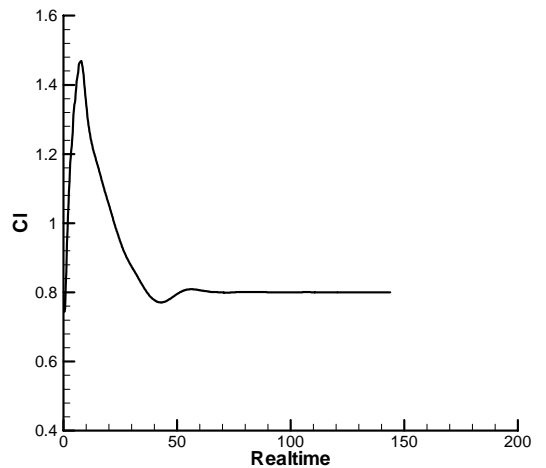


Fig. 13 Lift coefficient  $C_l$  evolution of  $Ma = 0.71$  and  $\alpha = 9.0^\circ$ .

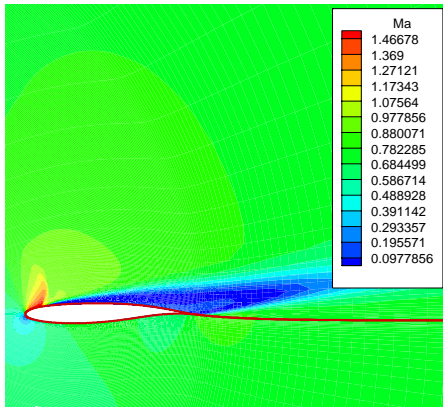


Fig. 14 Mach contour of  $Ma = 0.71$  and  $\alpha = 9.0^\circ$ .

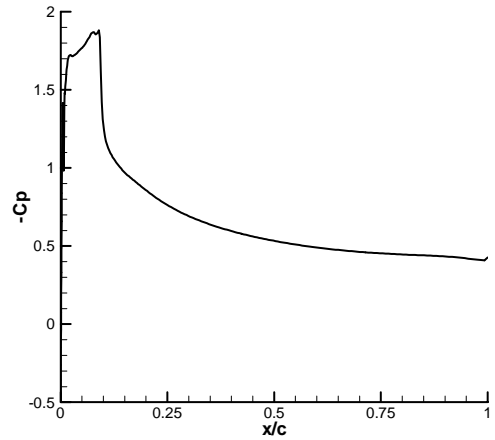


Fig. 15 Pressure distribution along the upper surface of airfoil.  $Ma = 0.71$  and  $\alpha = 9.0^\circ$ .

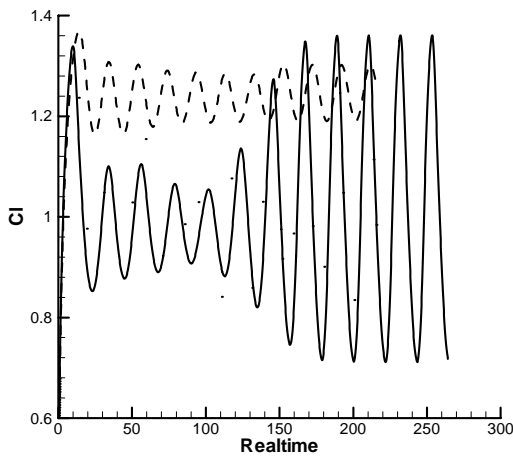


Fig. 16 Effect of mesh on lift coefficient  $C_l$  evolution for  $Ma = 0.71$  and  $\alpha = 6.97^\circ$ . Solid line: 640x64 grid; Dotted line: 552x48 grid; Dashed line: 320x32 grid.

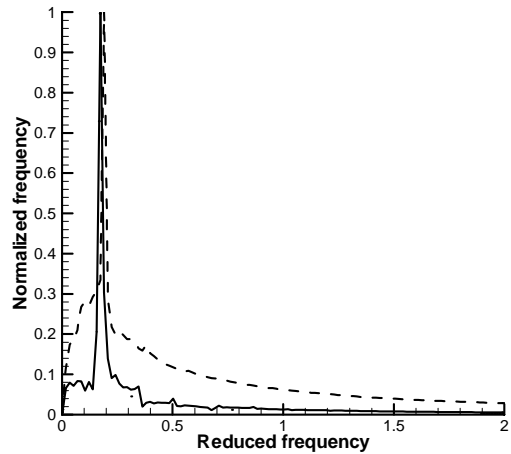


Fig. 17 Effect of mesh on the oscillation frequency. Solid line: 640x64 grid; Dotted line: 552x48 grid; Dashed line: 320x32 grid.

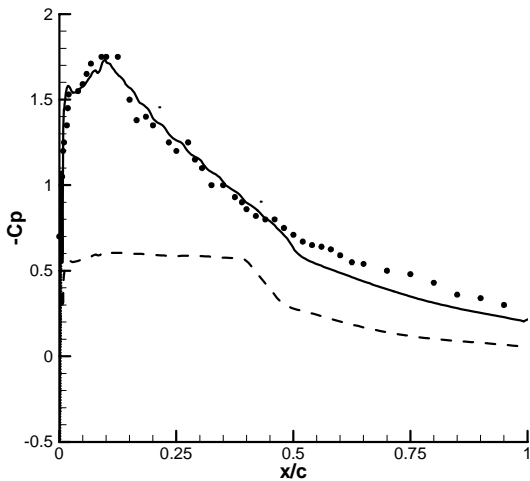


Fig. 18 Effect of mesh on the time-mean pressure distribution along the upper surface of airfoil. Solid line: 640x64 grid; Dotted line: 552x48 grid; Dashed line: 320x32 grid.

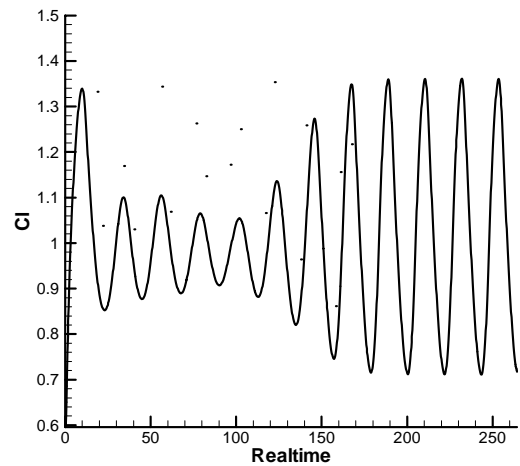


Fig. 19 Effect of initial condition on the lift coefficient  $C_l$  evolution. Solid line: start from uniform field; Dotted line: start from the converged steady solution.

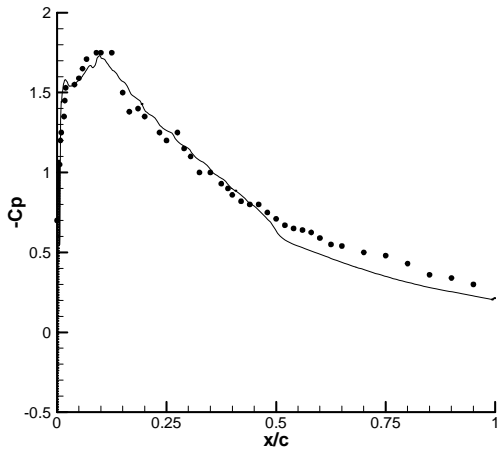


Fig. 20 Effect of initial condition on the lift coefficient  $C_l$  evolution. Solid line: start from uniform field; Dotted line: start from the converged steady solution.

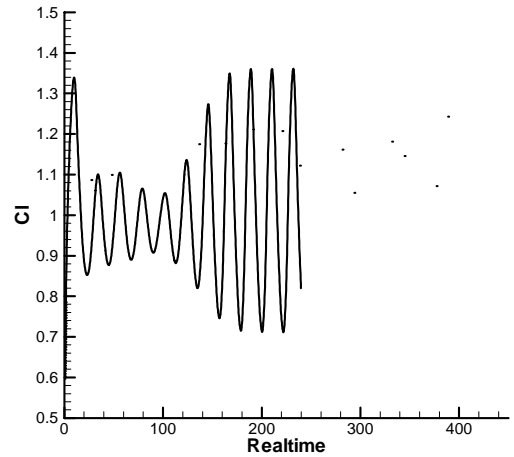


Fig. 21 Effect of lag model on lift coefficient  $C_l$  evolution for  $Ma = 0.71$  and  $\alpha = 6.97^\circ$ . Solid line: with the lag model; Dotted line: without the lag model.

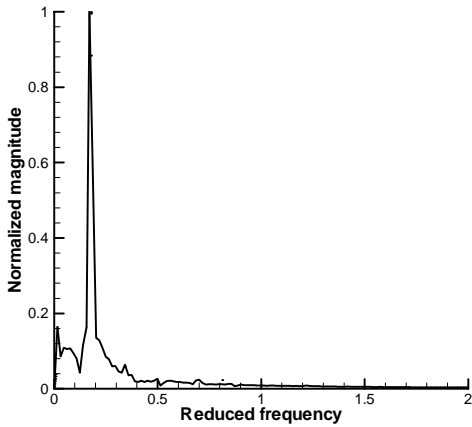


Fig. 22 Effect of lag model on the oscillation frequency. Solid line: with the lag model; Dotted line: without the lag model.

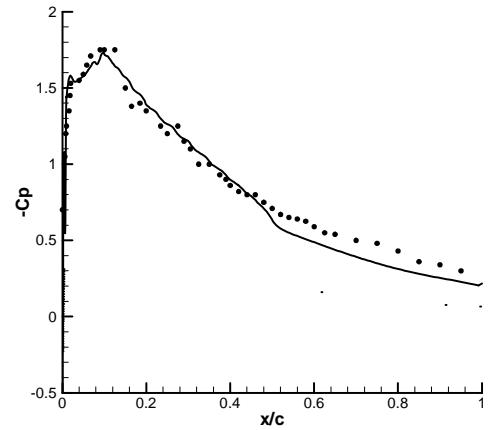


Fig. 23 Effect of lag model on the time mean pressure distribution along the upper surface of airfoil. Solid line: with the lag model; Dotted line: without the lag model; Circle: experiment.

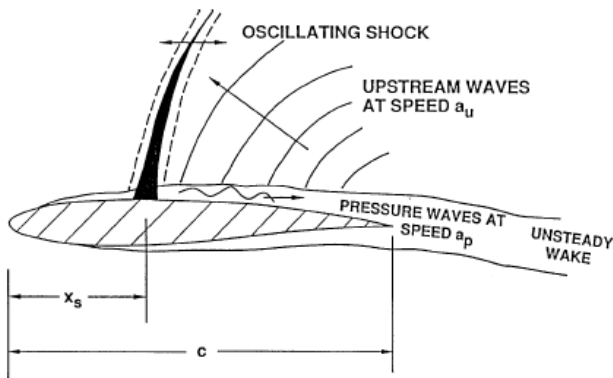


Fig. 24 Model of self-sustained oscillation. (From Ref. 12)



	A	B	C	D
$x/c$	1.0	0.795	0.591	0.5
$y/c$	0	0.0873	0.118	0.125

Fig. 25 Locations of the analysis for outside separation region cross-correlation.

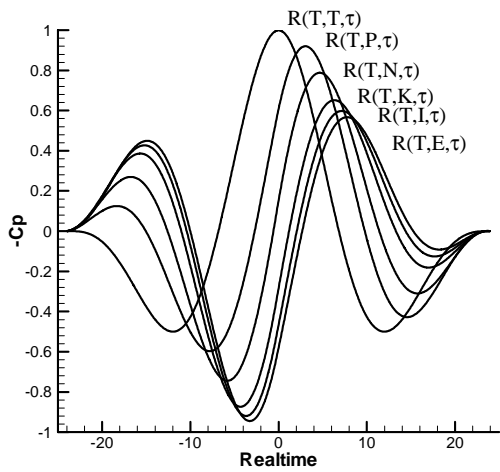


Fig. 26 Cross-correlation of computed unsteady pressure on airfoil, indicating downstream pressure wave inside the separation region.

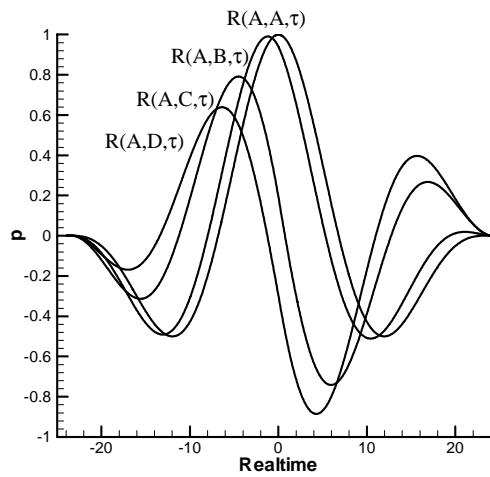


Fig. 27 Cross-correlation of computed unsteady pressure outside boundary-layer, indicating upstream propagating wave.

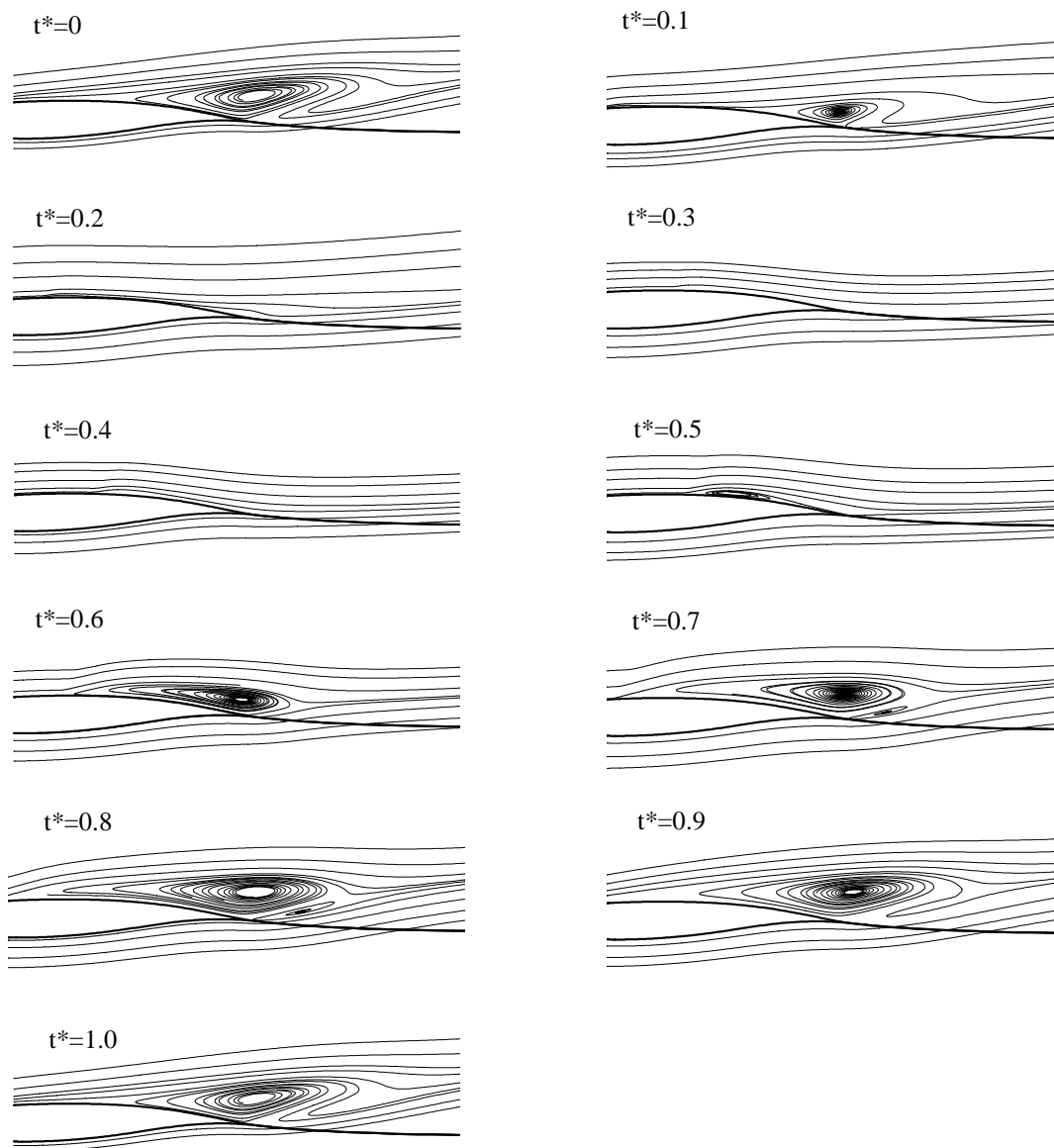


Fig. 28 Streamline plots at different instant time in one period.  $Ma = 0.71$  and  $\alpha = 6.97^\circ$ .